CCMS-84-10
VPI-84-24

VIRGINIA TECH

CENTER FOR COMPOSITE MATERIALS AND STRUCTURES

Free Edge Strain Concentrations in Real Composite Laminates: Experimental-Theoretical Correlation

C. T. Herakovich
D. Post
M. B. Buczek
R. Czarnek

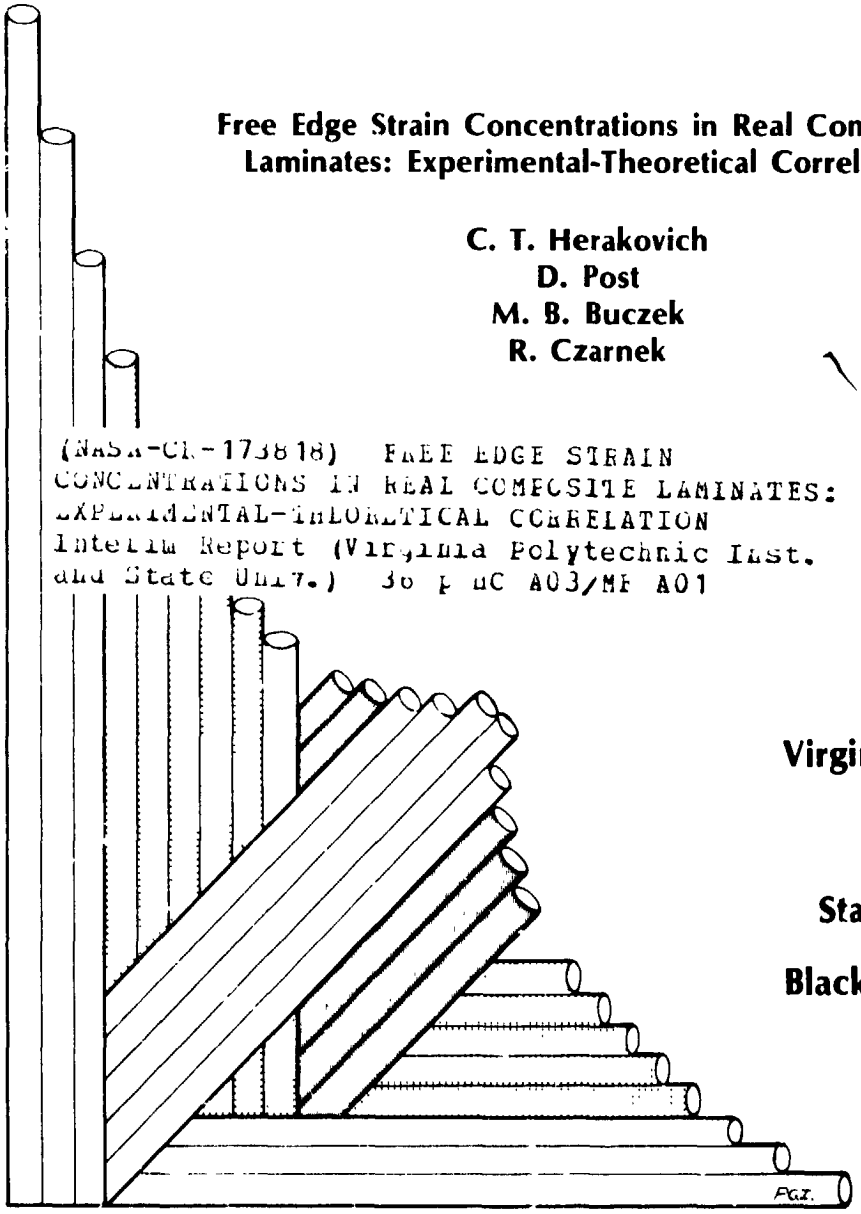

Virginia Polytechnic Institute and State University

Blacksburg, Virginia 24061

College of Engineering

Virginia Polytechnic Institute and State University

Blacksburg, VA 24061

VPI-E-84-24 July, 1984

Free Edge Strain Concentrations in Real Composite Laminates: Experimental-Theoretical Correlation

C. T. Herakovich[1]
D. Post[2]
M. B. Buczek[3]
R. Czarnek[4]

Department of Engineering Science & Mechanics

Interim Report 46
The NASA-Virginia Tech Composites Program

NASA Cooperative Agreement NCC1-15

Prepared for: Applied Materials Branch
National Aeronautics & Space Administration
Langley Research Center
Hampton, VA 23665

[1]Professor of Engineering Science & Mechanics

[2]Professor of Engineering Science & Mechanics

[3]Former Graduate Student, now Engineer with General Electric

[4]Graduate Student

ABSTRACT

The magnitude of the maximum shear strain at the free edge of axially loaded $[\theta_2/-\theta_2]_s$ and $[(\pm\theta)_2]_s$ composite laminates was investigated experimentally and numerically to ascertain the actual value of strain concentration in resin matrix laminates and to determine the accuracy of finite element results. Experimental results using moiré interferometry show large, but finite, shear strain concentrations at the free edge of graphite-epoxy and graphite-polyimide laminates. Comparison of the experimental results with those obtained using several different finite element representations showed that a four node isoparametric finite element provided the best and most trouble free numerical results. The results indicate that the ratio of maximum shear strain at the free edge to applied axial strain varies with fiber orientation and does not exceed nine for the most critical angle which is 15°.

INTRODUCTION

The problem of singular interlaminar stresses at the free edge of a finite width laminated composite structure has been under investigation continuously ever since the original paper of Pipes and Pagano [1]. Numerous papers have been published on the subject over the years. They have included the finite difference solution of Pipes and Pagano, approximate analytical solutions [2-4], finite element solutions [5-8], and several experimental investigations [9-11]. All theoretical investigations have modeled the laminate as combinations of distinct material layers with distinct interfaces. One paper modeled the interface as a separate layer, but still maintained distinct layer interfaces [12]. These papers have predicted large stress gradients in a boundary layer region along the free edges of laminated composites. The idealized model with distinct layers predicts singular interlaminar stresses at the free edge. Of prime importance to the designer are the magnitude and sign of the interlaminar stresses. High tensile interlaminar normal stresses and/or high interlaminar shear stresses can cause delamination failures at relatively low applied loads. This mode of failure is often the dominant mode and thus the great interest in this problem.

As depicted in Fig. 1, the real world is quite different from the idealized model that has been studied so extensively in the literature. Real laminates do not exhibit distinct interfaces between layers and hence the mathematical singularity is only an artifact of the idealized model. It is not present in the real world. This is, of course, borne out experimentally by the finite load required to initiate edge failure.

The studies that have been conducted on the idealized model have resulted in a clear understanding of the mechanics of the problem. They have shown the influence of material properties, fiber orientation and stacking sequence on the distribution of stresses in the boundary layer. Some analytical solutions have also provided results for the order of the singularity [4]. The insight that has been gained as a result of these studies is invaluable. However, failure analysis using these results is limited to the extent that the actual stresses in real composites are different from those predicted using an idealized, distinct interface model.

The intent of this paper is to present accurate experimental results for the maximum shear strain at the free edge for a family of angle-ply laminates and to compare the experimental results with finite element results obtained using a variety of element types and grids. Strains rather than stresses are emphasized in this paper because the moiré technique, which is used for the experimental measurements, provides displacements directly. The gradients of these displacements are the shear strains which can be compared with the strains obtained from the finite element solution. Stresses can be obtained with the appropriate constitutive equation, but this additional computation does introduce another degree of approximation due to the uncertainty associated with the elastic properties of composite materials (i.e., shear modulus and out-of-plane properties in particular).

A second goal of this investigation was to determine a suitable finite element representation for use in failure analysis of real world laminated composites. While the finite element method does not provide an exact solution to the idealized singular problem, it is possible to

obtain very accurate predictions of the "real world" strains using the finite element method. The difficulty lies in verification of a satisfactory element and grid. This can be determined only through comparison of theoretical and experimental results.

The experimental results in this paper were obtained using a high resolution moiré interferometry technique developed previously by one of the authors [13]. The finite element results were obtained using an existing code [5] and a program written specifically for this investigation by one of the authors (MBB). Experimental and numerical results were obtained for T300/5208 graphite-epoxy and Celion 6000/PMR-15 graphite-polyimide.

PROBLEM FORMULATION

The problem under consideration is depicted in Fig. 1. A long, finite width composite laminate is subjected to an imposed axial strain, ε_x. The laminate stacking sequence is symmetric about the midplane and balanced with plus and minus theta plies occurring in pairs (not necessarily adjacent). Under these conditions, stresses and strains away from the ends are independent of the axial coordinate x. In general, all six components of stress are non-zero. For thin laminates, the analysis may be restricted to one-quarter of the laminate cross-section [14].

This paper will consider only angle-ply laminates. Two stacking sequences are considered, $[\theta_2/-\theta_2]_s$ and $[(\pm\theta)_2]_s$. Fiber orientations of 10°, 30° and 45° were investigated experimentally. Finite element results were obtained at 10°, 15°, 20°, 25°, 30° and 45°. These fiber

orientations were chosen in order to survey the range from high to low interlaminar shear strains [15].

In displacement formulations of the finite element method, the fundamental unknowns of the problem are the element nodal point displacements. For the problem under consideration, a generalized plane strain assumption is made from which the most general form of the displacement field is:

$$\begin{aligned} u(x,y,z) &= U(y,z) + x\varepsilon_x \\ v(x,y,z) &= V(y,z) \\ w(x,y,z) &= W(y,z) \end{aligned} \tag{1}$$

Given ε_x, it is necessary to determine the unknown functions $U(y,z)$, $V(y,z)$ and $W(y,z)$. Four different isoparametric elements were used during the course of this investigation, the three node constant strain triangle, and four, eight and nine node quadrilateral elements. In all cases, minimization of the total potential energy for each element yields a set of simultaneous equations of the form

$$[K^{(e)}]\{U\} = \{F^{(e)}\} \tag{2}$$

where $[K^{(e)}]$ is the element stiffness matrix, $\{U\}$ is the nodal displacement vector, and $\{f^{(e)}\}$ is the element force vector. (The element stiffness matrix and force vector vary with the type of element [16]). The finite element equations (2) are assembled for all elements in the grid and the resulting set of simultaneous equations solved for the unknown nodal displacements.

Displacements at any location within an element can be determined using the element interpolation (shape) functions. Strains are then determined using the well-known strain-displacement relationships. The interlaminar shear strain γ_{xz} will be of prime consideration in this paper. The strain-displacement relationship for this component of strain is

$$\gamma_{xz} = \frac{\partial U}{\partial z} + \frac{\partial W}{\partial x} \tag{3}$$

However, W is independent of x for this problem and hence

$$\gamma_{xz} = \frac{\partial U}{\partial z} \tag{4}$$

Thus, the strain of interest at any location z on the free edge is equal to the through-the-thickness gradient of the U-displacement curve at that location.

EXPERIMENTAL PROGRAM

Moiré interferometry is a whole-field optical technique that produces contour maps (or fringe patterns) of in-plane displacement fields [13]. Its sensitivity is in the sub-wavelength range, viz. 0.417 μm (16.4μ in.) per fringe order for the current work, using a reference grating of 2400 lines/mm (60,960 ℓ/in.). The experimental techniques employed in this investigation are reported in Ref. [11]. Briefly, high frequency reflection gratings were applied to the face and edge of the laminate (Fig. 2a) by a relatively easy replication process. Those were viewed by an optical system that uses coherent laser light and produces patterns of in-plane displacements. Carrier patterns and optical fil-

tering were employed to cancel effects of initial fringes and yield patterns of the load-induced fringes exclusively.

The specimens were approximately 250 mm (10 in.) long, 12.5 mm (1/2 in.) wide and 1.0 to 1.3 mm (0.04 to 0.05 in.) thick. They were angle-ply laminates of graphite-epoxy and graphite-polyimide as specified above. The tensile loads were low, generating axial strains typically ranging about 0.05 percent for the $\pm 10°$ clustered laminate to a maximum of 0.2 percent for the $\pm 45°$ alternating laminate.

Moiré interferometry patterns are shown in Fig. 2b for edge views of $[\theta_2/-\theta_2]_s$ graphite/polyimide specimens. Face and edge views for graphite/epoxy specimens were shown in Ref. [11]. In all cases, the slopes of the fringes are fairly well defined at the locations where the fringes cross the $+\theta/-\theta$ interface. The relationship between this slope and the interlaminar shear strain γ_{xz} can be derived as follows.

At any point in the interference pattern, the fringe order, N_x, is related to the x-component of displacement, u, by

$$u = \frac{1}{f} N_x$$

where f is the frequency of the reference grating, here 2400 lines/mm. The displacement increment, Δu, between two points is proportional to the difference of fringe orders at the points, ΔN, viz.,

$$\Delta u = \frac{1}{f} \Delta N_x$$

Figure 3 is a schematic illustration of the fringes, with fringe orders enumerated as N_0 and $N_0 + 1$. A self-similar curve of fringe order

$N_o+1 - \Delta N$ can be drawn, where fractional fringe order ΔN can be as small as desired. At point A at the interface between cross-plies, the triangle ABC has leg AB = Δz and leg BC = $S\Delta N$. The latter is true because fringe orders change linearly with x in this problem, and therefore fractional distances are proportional to fractional fringe orders, or $BC/S = \Delta N/1$. Accordingly

$$\tan \phi = \frac{BC}{AB} = \frac{S\Delta N}{\Delta z} = Sf \frac{\Delta u}{\Delta z}$$

In the limit as ΔN approaches zero, and using Eq. 4

$$\tan \phi = Sf \frac{\partial u}{\partial z} = Sf\gamma_{xz} \tag{5}$$

The normal strain ε_x is

$$\varepsilon_x = \frac{\partial u}{\partial x} = \frac{1}{f} \frac{\partial N_x}{\partial x}$$

The gradient $\partial N_x/\partial x$ is a constant, namely one fringe per distance S, so

$$\varepsilon_x = \frac{1}{f} \left(\frac{1}{S}\right) \tag{6}$$

Thus, Eq. 6 can be written

$$\frac{\gamma_{xz}}{\varepsilon_x} = \tan \varphi \tag{7}$$

where ϕ is the angle of the tangent to the fringe, measured counterclockwise from the z-axis. This ratio is a measure of the strain con-

centration at the free edge and is of prime consideration in the investigation.

It is curious and helpful that fringe shape and ϕ are independent of ε_x [11]. As a consequence, small inadvertent bending that may have occurred in the experiment would cause ε_x to vary across the thickness of the specimen, but the angle ϕ would remain fixed.

RESULTS

Validity of the Finite Element Model

Qualitative comparisons of finite element predictions and moiré results for the through-the-thickness U-displacements at the free edge, Fig. 4, show that the finite element results give a good representation for the form of the actual displacement distributions. The mesh used for these results was an 896 element by 502 node grid of constant strain triangles. After imposing boundary conditions there were (1470) degrees of freedom (DOF). As indicated in Fig. 5a, this grid had a high density of small elements near the edge. There were 32 elements through the thickness of each layer at the free edge. The fringe lines of the moiré pattern correspond to lines of constant U-displacement. These results demonstrate that the finite element model exhibited the same trends as did the "real world" problem as recorded by the moiré fringe patterns, and that the initial assumption of x-independence (Eq. 1) is valid.

Element Dependence

A study was initiated to compare results from the constant strain triangle and several other isoparamentric elements. The additional

isoparametric elements chosen for study were four, eight and nine node elements. The grids for the eight and nine node element versions were identical 12 element meshes with the nine node version having an additional node in the interior of each element (Figs. 5b, 5c). There were 51 nodes in the eight node version and 63 nodes in the nine node version. One of two four-node element meshes used in the investigation (Fig. 5d) is identical to the nine node version, but with additional element sides connecting all interior node points. Thus, there are 63 nodes and 48 elements in this grid. The degrees of freedom are identical in this four and the nine node mesh (173), with the eight node mesh having fewer DOF (137). The quadrilateral isoparametric meshes (Figs. 5b-5d) are small modifications of the "optimal" mesh as given by Wang and Stango [17]. As with the constant strain triangular mesh, a higher density of smaller elements is used in the vicinity of the expected mathematical singularity.

Comparisons between finite element and classical lamination theory predictions for the axial stress, σ_{xx}, are presented in Table 1. The finite element results were taken from elements adjacent to the centerline (y=0) of the laminate. These results show that the eight node element with 137 DOF gave essentially exact results and the four node element with 173 DOF gave nearly exact results. The results from the nine node element were good (3 percent difference) for the 10° and 30° laminates, but, unexplainably, rose to 14 percent difference for the 45° laminate.

$[\theta_2/-\theta_2]_s$ Laminates

A primary concern of this investigation was to determine a satisfactory element and grid for accurate prediction of "real world" strains at the free edge of a laminate. A comparison of experimental and theoretical results for the distribution of shear strain through-the-thickness of the free edge of a $[30_2/-30_2]_s$ graphite-epoxy laminate is shown in Fig. 6. The theoretical results were obtained using four different isoparametric finite element representations. In addition to the three representations shown in Fig. 5b-5d, a dense mesh of four node rectangular elements (356 elements, 353 nodes and 1028 DOF) was used (Fig. 7). All theoretical and experimental results indicate that the maximum strain occurs at the interface between layers. As indicated in Fig. 5, the maximum strains from the numerical results varied considerably with the element and mesh used. The grid with 12 nine-node elements predicted maximum strains double the actual strains whereas the grid with 48 four-node elements predicted maximum strains 70 percent below the experimental values. The results from the grid of 12 eight-node elements and the 356 element grid of four-node elements were much closer to the actual strains. The maximum strain from the eight node element mesh was 20 percent higher than the actual value and the maximum strain using the four node mesh was 13 percent lower than the actual value. Thus, the best results were obtained with the 356 four-node rectangular element grid.

It is noted that the strains found in eight and nine node elements were first computed at the four Gauss stations used for a four node linear element and then linearly interpolated to any arbitrary point within the element. This interpolations was necessary to keep the

strains bounded when computing near the element corners of the eight and nine node elements. No such procedures were required with the four node elements, this is considered to be a sig ificant advantage of the four node element.

Figure 6 also shows that the maximum strain of the actual laminates did not occur at the exact quarter-point line of the specimen thickness. This was due to the fact that all layers of the actual laminate are not of equal thickness and thus the ± interface is not located exactly at the quarter-point as in the idealized model. The maximum strain did occur at the ± interface.

A summary of experimental and numerical results for the maximum free-edge shear strains at the +θ/-θ interface of $[\theta_2/-\theta_2]_s$ laminates is presented in Table 2 and Fig. 8. The finite element results were obtained using the 356 element grid of rectangular elements. They indicate that the largest strain concentration occurs at approximately 15° for both graphite-epoxy and graphite-polyimide; the maximum strain concentration factors are 7.9 and 8.9, respectively. The numerical results for the two materials show very similar trends. The strains in the graphite-polyimide are significantly higher than those in the graphite-epoxy in the 10°-30° fiber orientation range. This difference is because the two materials have different material properties (Table 3).

The experimental results indicate trends similar to the finite element results. Unfortunately, experimental results were not obtained for the most critical fiber orientation. The maximum measured strain concentration $\gamma_{xz}/\varepsilon_x$ was 5.9 for the 30° graphite-epoxy specimen. However, this value is not significantly greater than the 5.3 value for the 10° laminate. The measured strain concentrations were lower than

the predicted values in all cases with the difference being largest at the lower fiber angles. It is interesting to note that theory predicts higher strains in the polyimide, but experiment indicates higher strains in the epoxy. This is a clear indication that the input data to the analysis are not an exact representation of the experiment. Materials properties as well as individual layer thicknesses may be in error.

The slopes of fringes at the $+\theta/-\theta$ interface were found to vary for different fringes in the same specimen. Seven patterns were analyzed--four in addition to the three shown in Fig. 2b. The variation is attributed partly to experimental error in determining the slope and partly to point-to-point variations in the specimen material. Table 4 shows the variations attributed to experimental error and the variations attributed to material variations. The material variations appear to be significantly large. Another factor is the difference of fringe slope on the left and right interfaces of the laminate, which verifies the specimen nonuniformity and adds to the variations reported in Table 4.

$[(\pm\theta)_2]_s$ Laminates

The results of the previous section have shown that the dense four-node rectangular element mesh of Fig. 7 provides reasonably good correlation between theory and experiment for the free edge shear strains in $[\theta_2/-\theta_2]_s$ laminates. Additional evidence from other laminates is necessary before this mesh can be accepted with confidence.

Figure 9 shows moiré fringe patterns for $[(\pm\theta)_2]_s$ graphite-epoxy laminates. The corresponding displacements from the four-node, 356 element mesh are presented in Fig. 10. Comparison of the figures indicates good correlation between theory and experiment.

Results for strain concentrations $\gamma_{xz}/\varepsilon_x$ at the free edge of the $[(\pm\theta)_2]_s$ laminates are presented in Table 4 and Fig. 11. These results show that this mesh also provides very good correlation with experiment for the alternating layer stacking sequence. The experimental values in Table 4 are the average from several fringes (4-10) along the length of the specimens. Strain concentrations were determined at each interface (numbered 1-6). It is apparent from the table that the experimental results did not always exhibit symmetric response about the specimen midplane. (The results along a given interface were quite consistent.) The largest differences occurred between the two outermost layers. It is believed that these differences are due to the lack of exact symmetry in the actual specimens. (Experimental error in measuring the strains was discussed previously.)

The average values from both sides of the midplane indicate very good correlation between theory and experiment. In all but two cases the percent difference was less than 14 percent. The maximum difference between average measured value and finite element value was 41 percent.

Comparison of finite element results for the clustered $[\theta_2/-\theta_2]_s$ and the alternating $[(\pm\theta)_2]_s$ laminates indicates that the clustered laminates should exhibit higher strain concentrations for the corresponding fiber orientations. This was generally (but not always) the case for the experimental results.

CONCLUSIONS

Experimental results have been presented showing that the maximum shear strains on the free edge of angle-ply laminates are finite. Measured values for the ratio of maximum edge shear strain to applied

axial strain did not exceed 7.5 for $[\theta_2/-\theta_2]_s$ and $[(\pm\theta)_2]_s$ laminates. Numerical analysis indicates that the maximum strain concentration for angle-ply laminates would not exceed 9.0 for resin matrix laminates.

Comparison of finite element and experimental results indicates that the most satisfactory and trouble free numerical results were obtained with a four node, isoparametric, rectangular element mesh. Good comparison between theory and experiment was obtained for both $[\theta_2/-\theta_2]_s$ and $[(\pm\theta)_2]_s$ laminates using the identical mesh. Experimental results show that there is considerable variation in strains along the length and through the thickness of real laminates. These variations are an indication of nonuniformity in the fabricated laminates.

ACKNOWLEDGEMENT

This work was supported by the NASA Cooperative Agreement NCC1-15 and NSF Grant MEA 8109230. The authors are also grateful for the assistance of Mr. Duksong Joh with data reduction.

REFERENCES

1. Pipes and Pagano, "Interlaminar Stresses in Composite Laminates Under Uniform Axial Extension," J. Composite Materials, Vol. 4 (Oct), 1970, pp. 538-548.

2. Hsu, P. W. and Herakovich, C. T., "Edge Effects in Angle-Ply Composite Laminates," Journal of Composite Materials, Vol. 11, Oct. 1977, pp. 422-428.

3. Pagano, N. J., "Free-Edge Stress Fields in Composite Laminates," Int. J. Solids & Structures, Vol. 14, 1978, pp. 401-406.

4. Wang, S. S., and Choi, I., "Boundary-Layer Effects in Composite Laminate: Part 2--Free-Edge Stress Solutions and Basic Characteristics," J. Applied Mechanics, Sept. 1982, Vol. 49, pp. 549-560.

5. Herakovich, C. T., Renieri, G. D., and Brinson, H. F., "Finite Element Analysis of Mechanical and Thermal Edge Effects in Composite Laminates," Army Symposium on Solid Mechanics, 1976, Composite

Materials: The Influence of Mechanics of Failure on Design, Cape Cod, MA, Sept. 1976, pp. 237-248.

6. Renieri, G. D. and Herakovich, C. T., "Nonlinear Analysis of Laminated Fibrous Composites," VPI-E-76-10, June 1976, 177 pages.

7. Wang, A. S. D., and Crossman, F. W., "Some New Results on Edge Effects in Symmetric Composite Laminates," J. Composite Materials, Vol. 11, (January) 1979.

8. Rybicki, E. F., "Approximate Three-Dimensional Solutions for Symmetric Laminates Under In-Plane Loading," J. Composite Materials, Vol. 5, July 1971, pp. 354-360.

9. Pipes, R. B. and Daniel, I. M., "Moiré Analysis of the Interlaminar Shear Edge Effect in Laminated Composites," J. Composite Materials, Vol. 5 (April) 1971, p. 255.

10. Oplinger, D. W., Parker, B. S., and Chiang, F. P., "Edge-Effect Studies in Fiber-Reinforced Laminates," Experimental Mechanics, Vol. 14, No. 9, (Sept) 1974, pp. 347-354.

11. Czarnek, R., Post, D. and Herakovich, C. T., "Edge Effects in Composites by Moire Interferometry," Experimental Techniques, 7(1), 18-21 (Jan. 1983).

12. Puppo, A. H. and Evensen, H. A., "Interlaminar Shear in Laminated Composite Under Generalized Plane Stress," J. Composite Materials, Vol. 4, 1970, pp. 204-220.

13. Post, D., "Moire Interferometry at VPI & SU," Experimental Mechanics, 23(2), 203-210 (June 1983).

14. Griffen, O. H., Kamat, M. P. and Herakovich, C. T., "Three Dimensional Inelastic Finite Element Analysis of Laminated Composites," VPI-E-80-28, Virginia Tech, November 1980, 169 pages.

15. Herakovich, C. T., "On the Relationship Between Engineering Properties and Delamination of Composite Materials," J. Composite Materials, Vol. 15, July 1981, pp. 336-348.

16. Reddy, J. N., An Introduction to the Finite Element Method," McGraw-Hill Co., New York, NY, 1984.

17. Wang, S. S. and Stango, R. J., "Optimally Discretized Finite Elements for Boundary-Layer Stresses in Composite Laminates," AIAA 82-0748-CP, 23rd Structures, Structural Dynamics and Materials Conference, May 11-12, 1982, New Orleans.

TABLE 1

Comparison of Lamination Theory and Finite Element Results (ε_x = 0.1%)

Laminate	Normal Stress σ_x (x,y = 0, z = 0) (ksi/MPa)				
	Lamination Theory	Constant Strain Triangle	4-Node Elements	8-Node Elements	9-Node Elements
$[10_2/-10_2]_s$	17.6/121	17.8/123	17.8/123	17.6/121	17.1/118
$[30_2/-30_2]_s$	7.1/49	7.3/50	7.3/50	7.1/49	6.9/48
$[45_2/-45_2]_s$	2.8/19	2.8/19	2.8/19	2.8/19	2.4/17

T300/5208 Gr/Ep

TABLE 2

Comparison of Finite Element Results with Experiment for Interfacial Shear Strain Concentrations $\gamma_{xz}/\varepsilon_x$ in Clustered Laminates

Laminate	Interfacial Shear Strains Concentrations $\gamma_{xz}/\varepsilon_x$			
	Graphite-Epoxy		Graphite-Polyimide	
	4-Node F.E.	Experiment	4-Node F.E.	Experiment
$[10_2/-10_2]_s$	7.0	6.0	7.9	4.1*
$[15_2/-15_2]_s$	8.1	---	8.9	---
$[20_2/-20_2]_s$	8.0	---	8.7	---
$[25_2/-25_2]_s$	7.3	---	7.7	---
$[30_2/-30_2]_s$	6.1	5.9	6.3	5.1
$[45_2/-45_2]_s$	2.8	1.0	2.7	2.2

*Small fiber misalignment during fabrication

TABLE 3

Elastic Properties for Graphite-Epoxy
and Graphite-Polyimide

Property	T300/5208 Gr/Ep	Celion 6000/PMR-15 Gr/Pi
E_1(GPa)	132.0	136.0
E_2(GPa)	10.8	9.79
E_3(GPa)	10.8	9.79
ν_{23}	0.490	0.49
ν_{13}	0.238	0.35
ν_{12}	0.238	0.35
G_{23}(GPa)	3.36	3.36
G_{13}(GPa)	5.65	5.00
G_{12}(GPa)	5.65	5.00

TABLE 4

Experimental Results for Clustered Laminates
Including Variations and Error

Specimen	ϕ	$\gamma_{xz}/\varepsilon_x$	Max. Variation in ϕ *	Max. Expml. Error **	$\Delta\phi$ ***	
					Min.	Max.
Gr/Ep $[10_2/-10_2]_s$	80.5°	6.0	2.7°	1°	1.7°	3.7°
Gr/Pi $[10_2/-10_2]_s$	76.3	4.1	1.0	1	0	2
Gr/Pi $[30_2/-30]_s$	78.8	5.1	1.4	1	0.4	2.4
Gr/Pi $[45_2/-45_2]_s$	65.4	2.2	6	3	3	9

*Averaged for interfaces on left and right side.

**Estimated

***Minimum and maximum variation in ϕ attributable to variations in local specimen properties and dimensions.

TABLE 5

Theoretical-Experimental Correlation of Strain Concentrations for Alternating Laminates

Laminate	INTERFACE					
	1	2	3	4	5	6
	MAGNITUDE OF EXPERIMENTAL γ_{xz}/ϵ_x					
$[(\pm 10)_2]_s$	5.2	4.4	6.8	6.0	4.3	7.2
Avg			6.4			
Avg		4.35				
Avg	6.2					
$[(\pm 30)_2]_s$	3.6	2.4	4.5	5.0	2.9	4.6
Avg			4.75			
Avg		2.65				
Avg	4.1					
$[(\pm 45)_2]_s$	1.7	1.0	2.2	2.0	1.0	2.0
Avg			2.1			
Avg		1.0				
Avg	1.85					
	MAGNITUDE OF THEORETICAL γ_{xz}/ϵ_x					
$[(\pm 10)_2]_s$	5.6	4.1	5.6	5.6	4.1	5.6
$[(\pm 30)_2]_s$	4.7	3.6	4.8	4.8	3.6	4.7
$[(\pm 45)_2]_s$	2.1	1.7	2.2	2.2	1.7	2.1

T300/5208

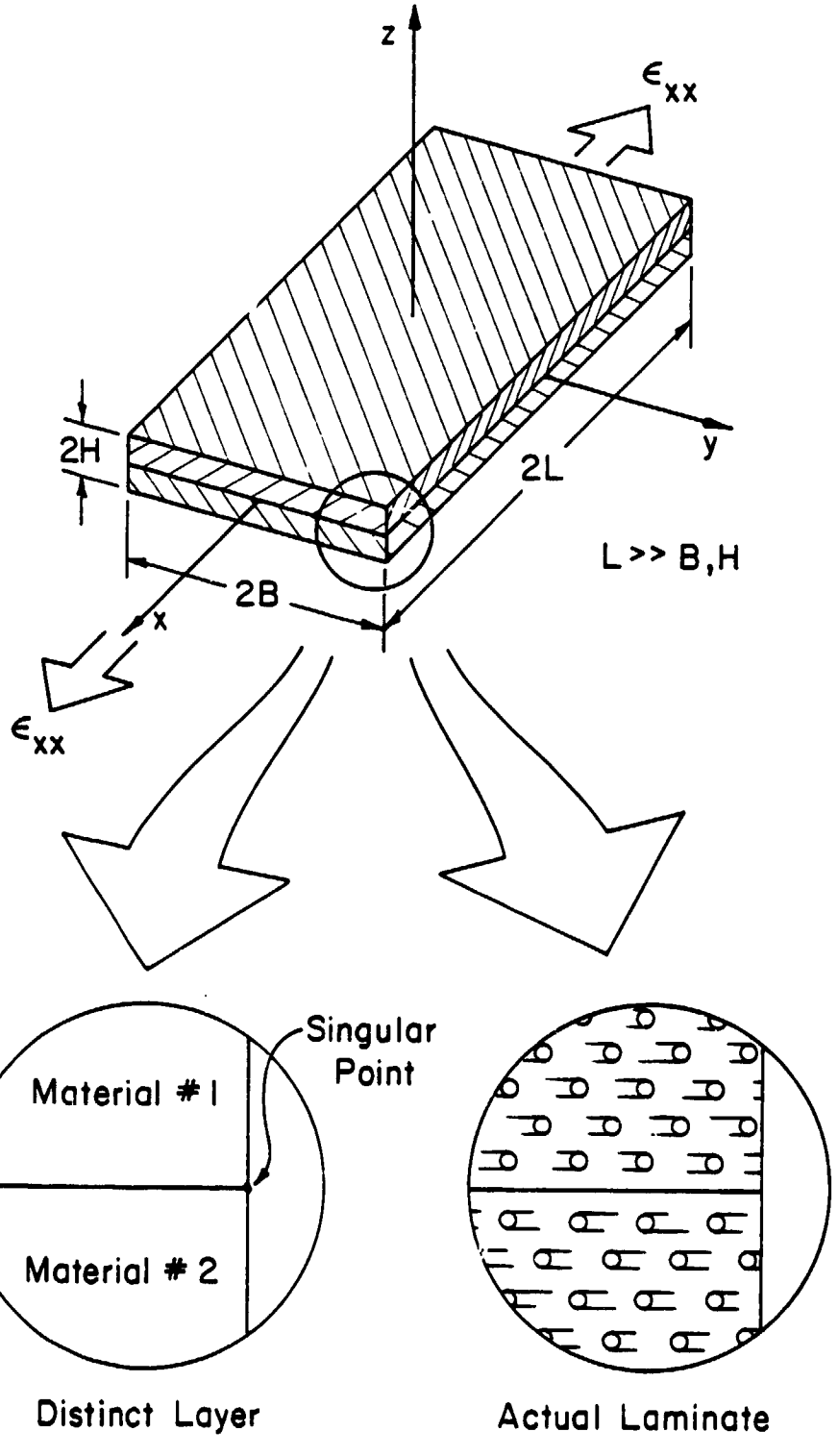

FIG. 1. Distinct Layer Interface and Actual Laminate Interface.

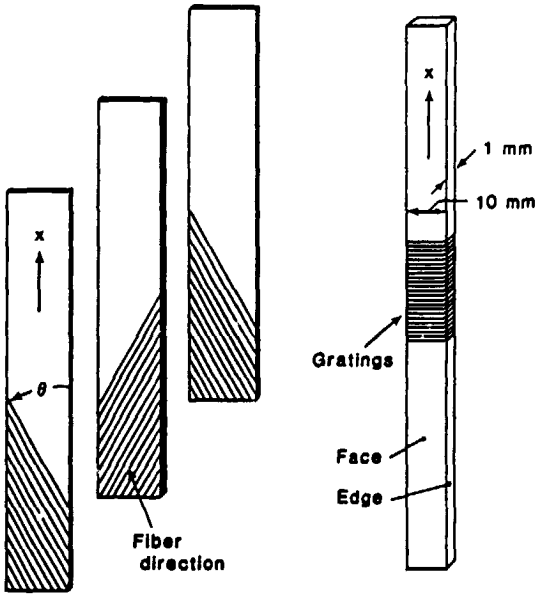

a) Specimens and Gratings

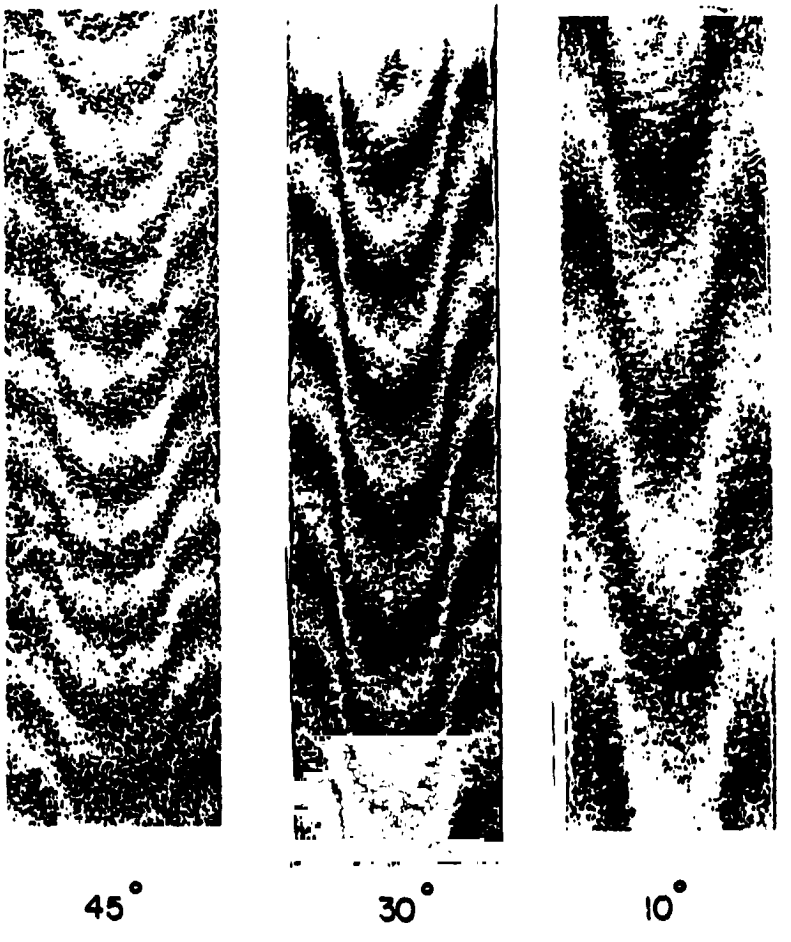

b) Fringe Patterns for $[\theta_2/-\theta_2]_s$ Laminates

FIG. 2. Moire Fringe Patterns

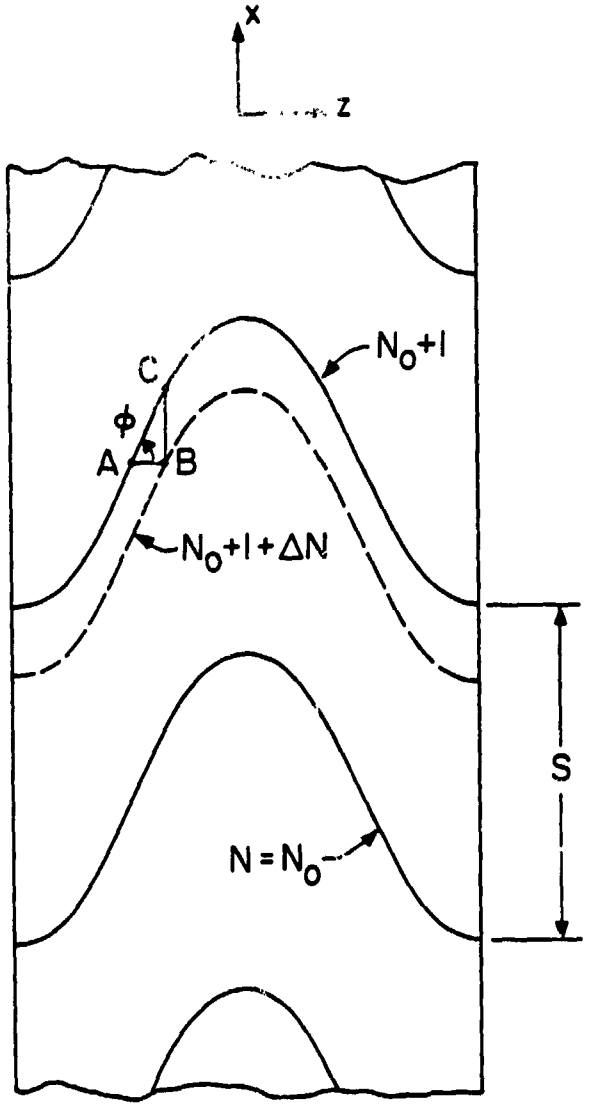

FIG. 3. Typical Fringe Pattern for $[\theta_2/-\theta_2]_s$ Laminate.

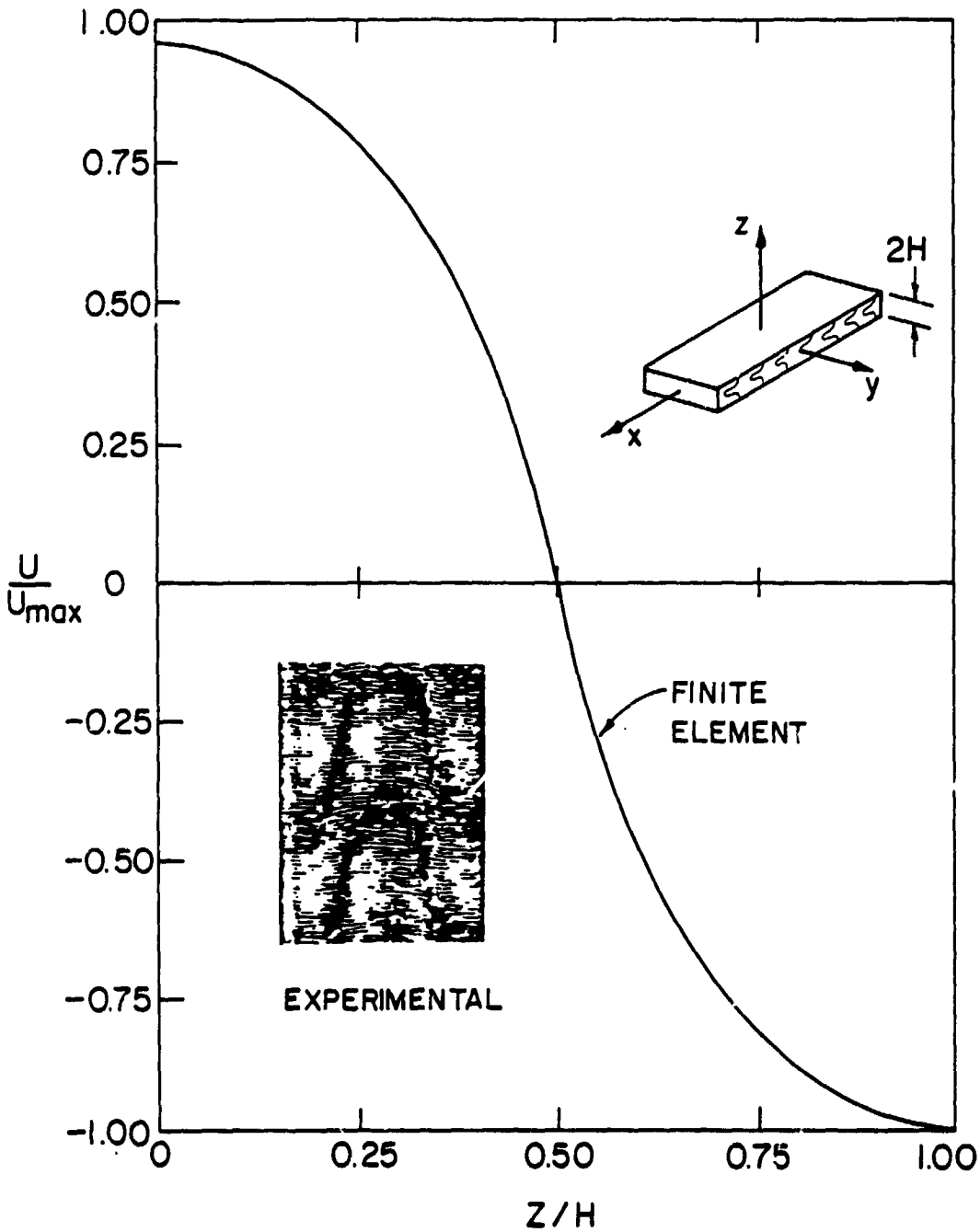

FIG. 4. Experimental and Finite Element Free Edge U Displacements for a $[30_2/-30_2]_s$ Laminate.

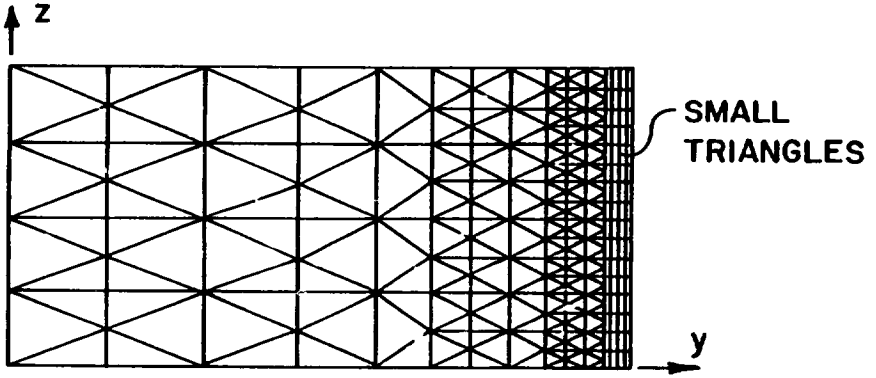

a) TRIANGULAR MESH
(896 ELEMENTS, 502 NODES, 1470 DOF)

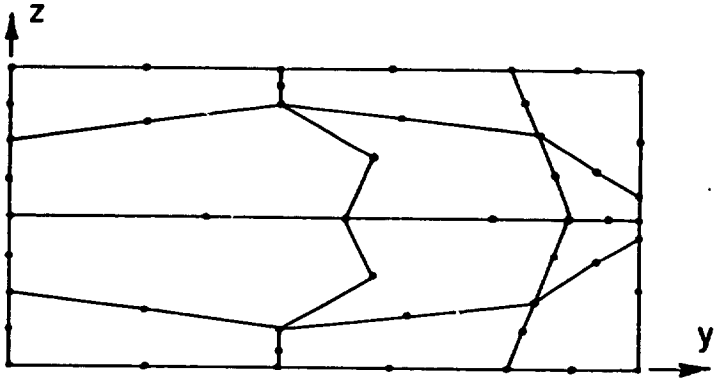

b) EIGHT NODE ELEMENT MESH
(12 ELEMENTS, 51 NODES, 136 DOF)

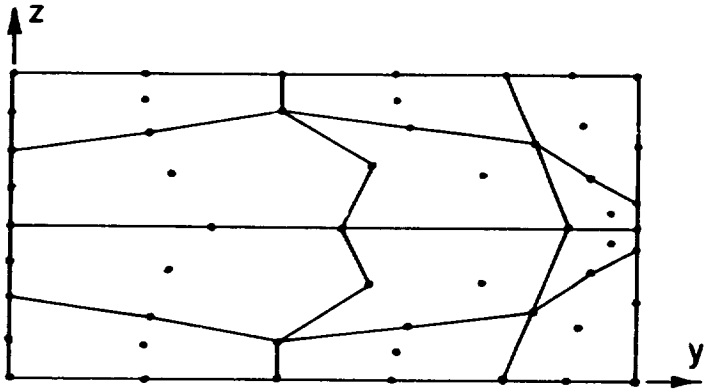

c) NINE NODE ELEMENT MESH
(12 ELEMENTS, 63 NODES, 173 DOF)

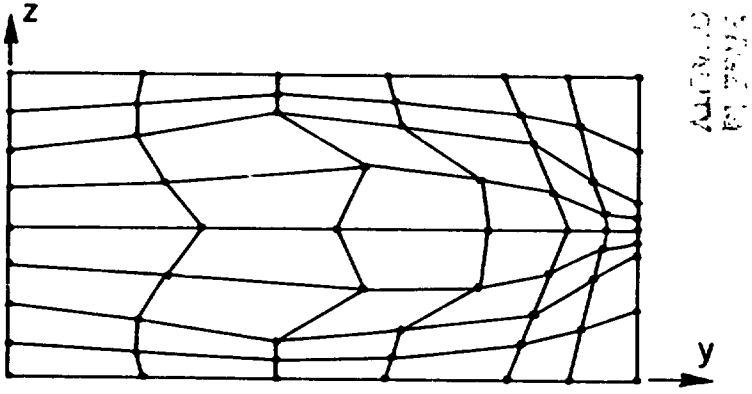

d) FOUR NODE ELEMENT MESH
(48 ELEMENTS, 63 NODES, 173 DOF)

FIG. 5. Finite Element Representations for $[\theta_2/-\theta_2]_s$ Laminates.

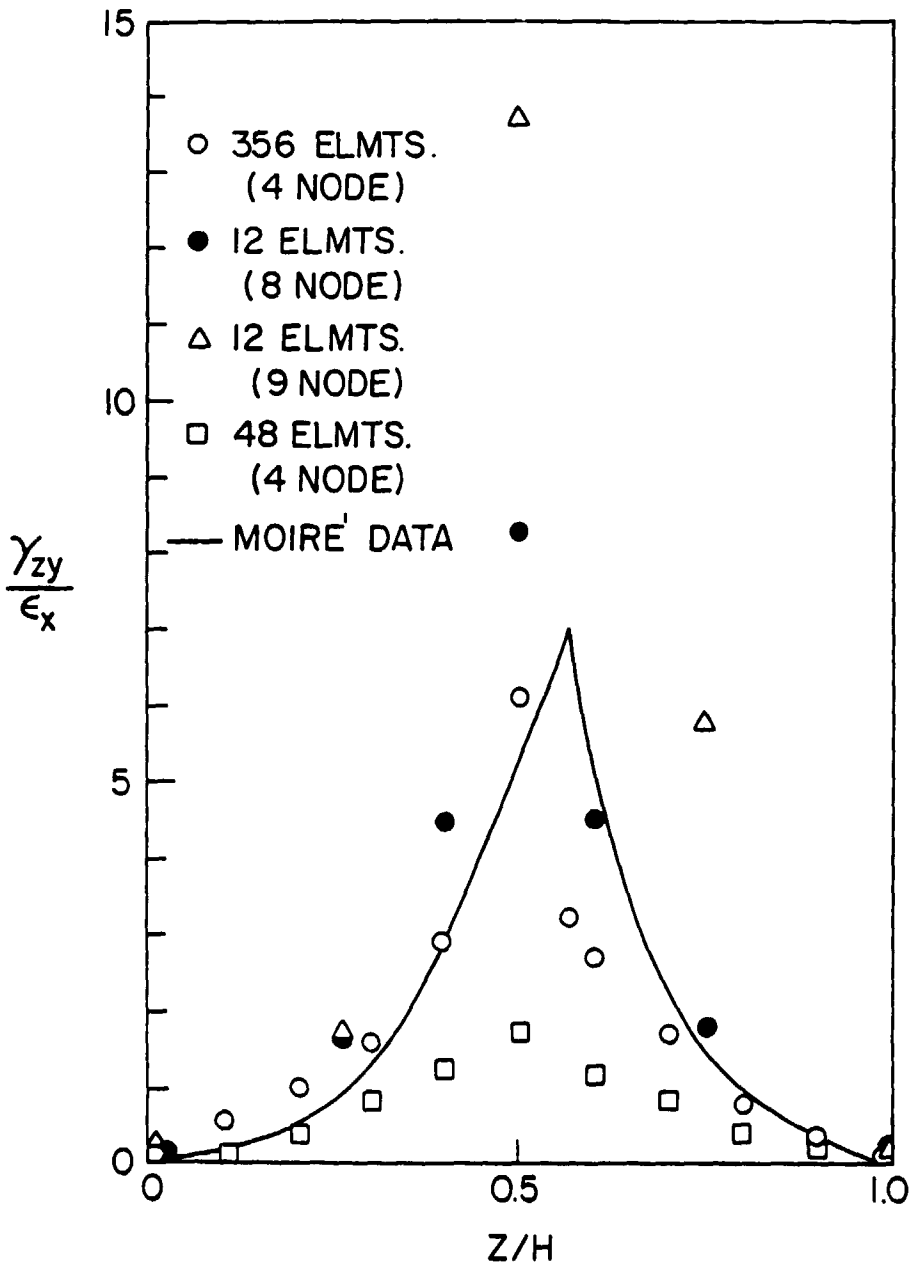

FIG. 6. Strain Concentration on Free Edge of $[30_2/-30_2]_s$ Laminate.

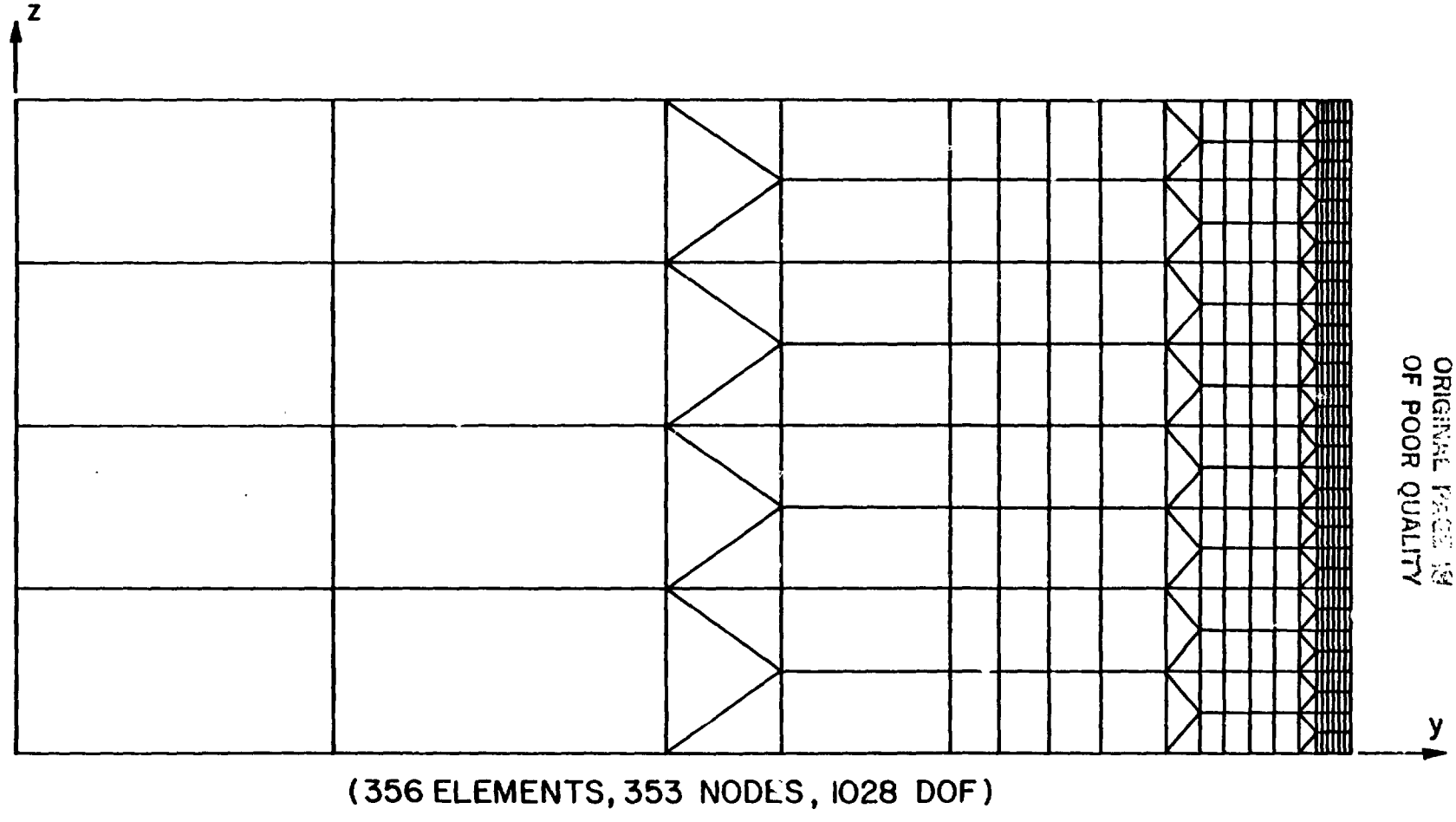

FIG. 7. Dense 4-Node Rectangular Element Mesh.

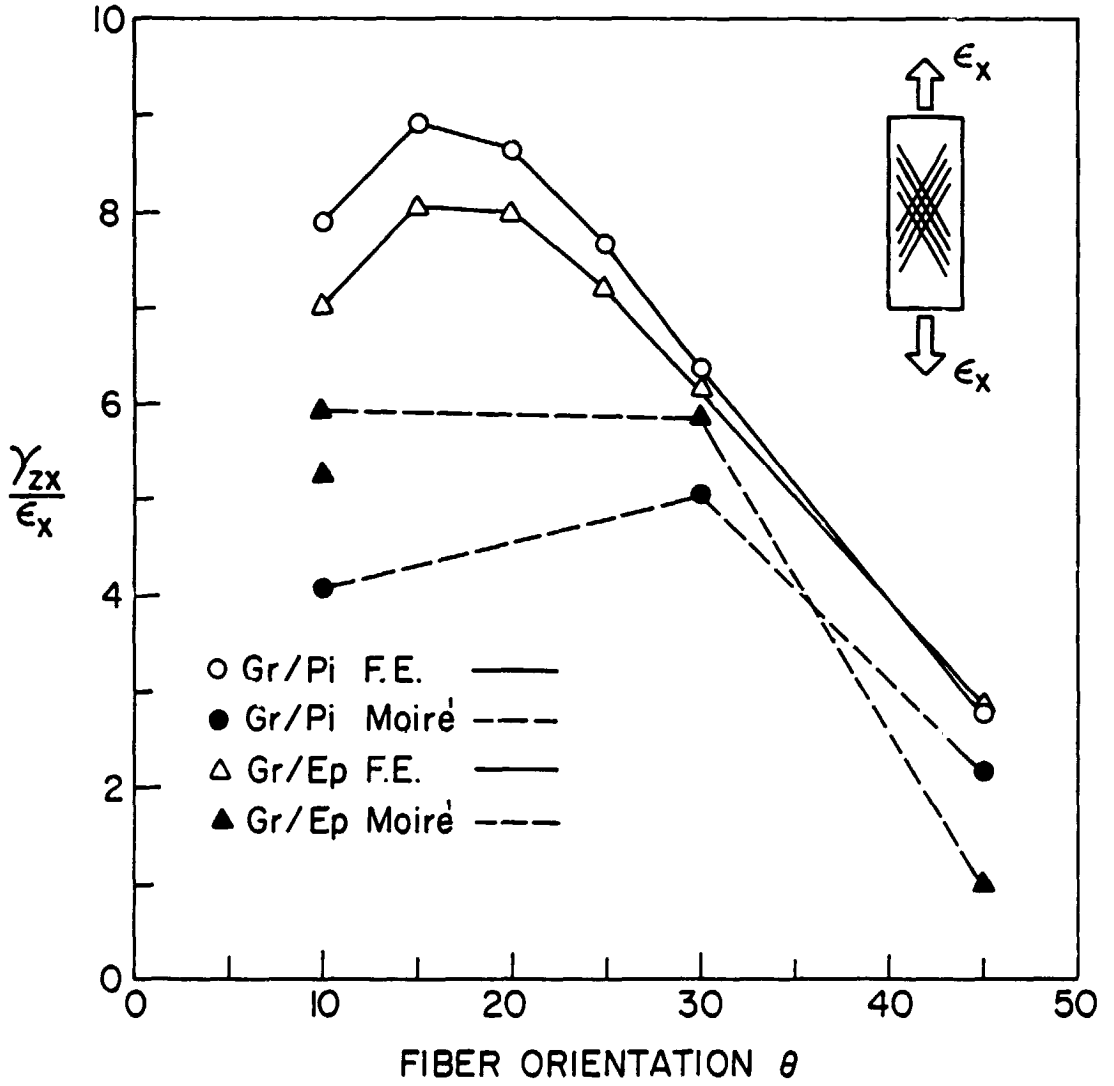

FIG. 8. Theoretical/Experimental Correlation for Maximum Strain Concentrations on Free Edge of $[\theta_2/-\theta_2]_s$ Laminates.

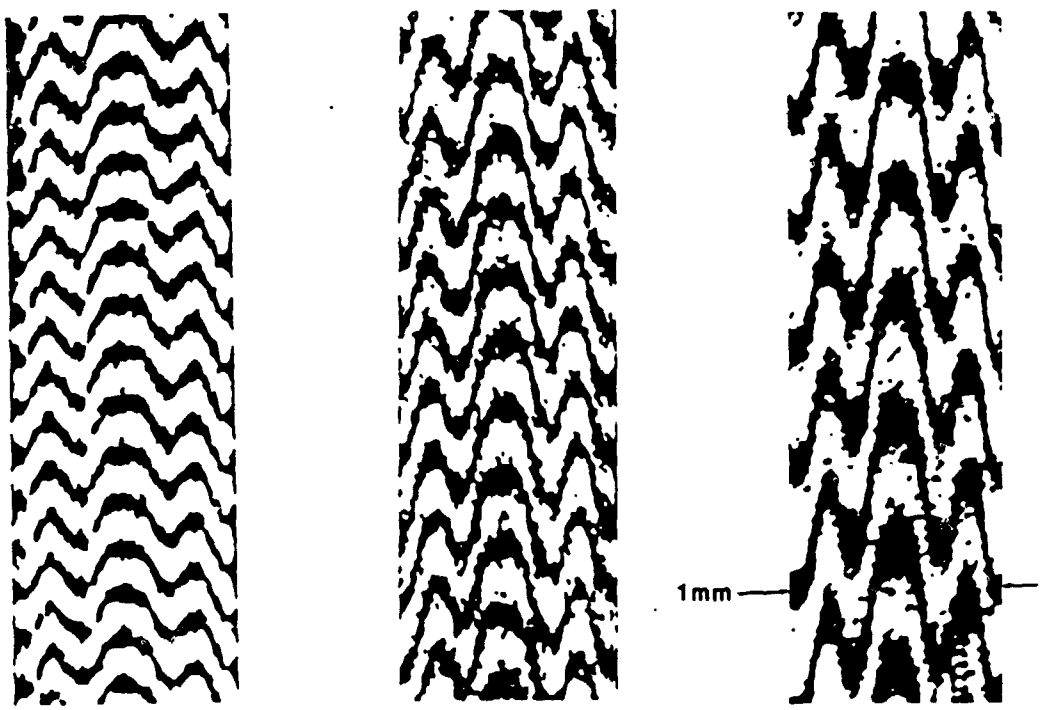

FIG. 9. Moire Fringe Patterns for $[(\pm\theta)_2]_s$ Laminates.

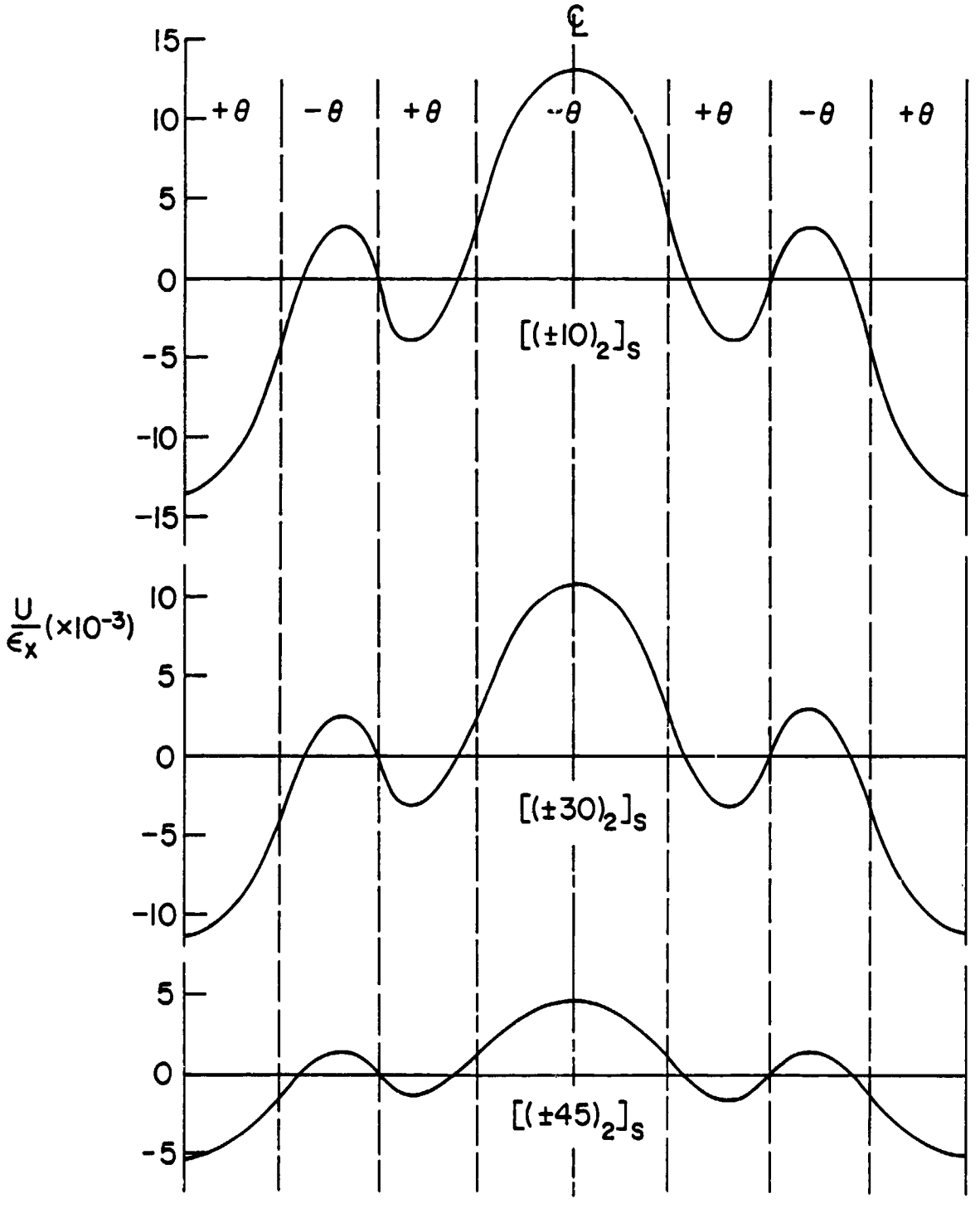

FIG. 10. Theoretical U Displacements on Free Edge of $[(\pm\theta)_2]_s$ Laminates.

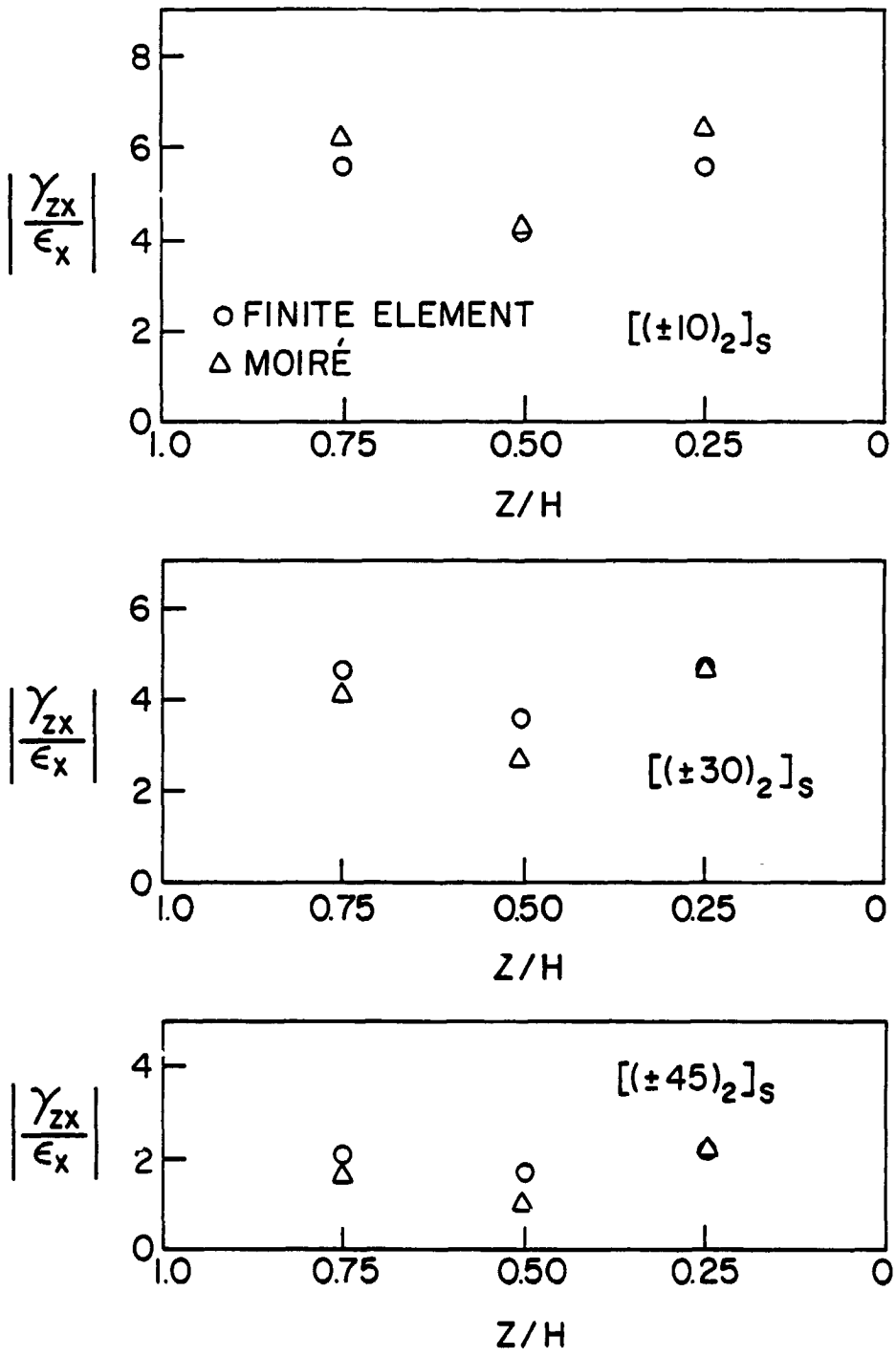

FIG. 11. Theoretical/Experimental Correlation for Free Edge Strain Concentrations in $[(\pm\theta)_2]_s$ Laminates.